Applied Catalysis B: Environmental 156–157 (2014) 8–14

Contents lists available at ScienceDirect

Applied Catalysis B: Environmental

journal homepage: www.elsevier.com/locate/apcatb

A TiO_2 surface modified with copper(II) phthalocyanine-tetrasulfonic acid tetrasodium salt as a catalyst during photoinduced dichlorvos mineralization by visible solar light

Estrella Vargas [a,b], Ronald Vargas [c], Oswaldo Núñez [a,*]

[a] Laboratorio de Fisicoquímica Orgánica y Química Ambiental, Departamento de Procesos y Sistemas, Universidad Simón Bolívar, Apartado 89000, Caracas 1080A, Venezuela
[b] Escuela de Química, Facultad de Ciencias, Universidad Central de Venezuela, Caracas, Venezuela
[c] Laboratorio de Electroquímica, Departamento de Química, Universidad Simón Bolívar, Apartado 89000, Caracas 1080A, Venezuela

ARTICLE INFO

Article history:
Received 29 October 2013
Received in revised form 20 February 2014
Accepted 25 February 2014
Available online 5 March 2014

Keywords:
TiO_2 Degussa P25
Copper(II) phthalocyanine-tetrasulfonic acid tetrasodium salt (CuPc)
Dichlorvos (2,2-dichlorovinyl dimethyl phosphate) (DDVP)
Visible light
Bell shape
Rate vs. C_{DDVP} profile.

ABSTRACT

Two consecutive Langmuir isotherms were used in this study to describe copper(II) phthalocyanine-tetrasulfonic acid-tetrasodium salt (CuPc) adsorption by TiO_2-Degussa-P25. UV–vis reflectance spectroscopy confirmed CuPc adsorption on the TiO_2 surface. FTIR spectra revealed less TiO–sulfonic interactions for maximum CuPc surface coverage (39 mg g^{-1}) of the second Langmuir than the maximum coverage (8 mg g^{-1}) of the first Langmuir. This finding indicates that there is more than one TiO–sulfonic interaction per CuPc molecule. Dichlorvos (DDVP)-water solutions were degraded with the modified TiO_2 catalyst and visible simulated solar light. The highest degradation rates were obtained using 8 mg g^{-1} CuPc at a neutral pH with a maximum k_{obs} = 0.0072 min^{-1}. Under this condition, a rate vs. DDVP concentration (C_{DDVP}) bell-shaped profile was observed. This tendency can be explained in terms of dissolved oxygen singlet formation via visible light surface sensitization. This process was diminished at high C_{DDVP} because of DDVP competition with dissolved oxygen to reach the catalyst surface. DDVP degradation and mineralization have the same rate limiting step. Therefore, there is no intermediate accumulation during treatment. The modified TiO_2-CuPc catalyst activity was further improved when solar simulated light (including UV) was used to degrade DDVP. In fact, the fastest degradation rate constant (k_{obs} = 0.011 min^{-1}) was obtained using high CuPc coverage (39 mg g^{-1}).

1. Introduction

Heterogeneous photocatalysis with TiO_2 and ultraviolet solar radiation is one advanced oxidation process (AOP) for removing organic compounds from contaminated water. In this process, hydroxyl radicals promote organic matter oxidation [1–4]. This technology is quite attractive because solar energy radiation is used to initiate organic matter degradation (solar detoxification) [5–7]. Under conditions of TiO_2/UV light photocatalysis, an electron from the TiO_2 valence band is promoted to the conduction band, generating a hole in the valence band (h_{VB}^+) and an electron in the conduction band (e_{CB}^-). These holes can react directly with organic substrates to generate free radicals. They can also be trapped by water or hydroxyl anions to form hydroxyl radicals. Electrons in the conduction band can react with dissolved oxygen to form a superoxide radical, which can then be trapped by water to form a peroxide that decomposes into more hydroxyl radicals [2,3,7–9]. Radicals that form on the TiO_2 surface are highly reactive and generally promote organic substrate oxidation via hydrogen abstraction, addition to double bonds or aromatic rings [8].

In recent years, efforts have been directed for increasing the TiO_2 spectral range by means of incorporating visible light activity (the amount of solar irradiance on earth in the UV range is less than 5% and the quantity in the visible range is ca. 45%). Some examples of these efforts are the sensitization of semiconductors using an organic molecule that absorbs visible radiation [9–14], the anchoring of "organic molecular wire" to extend the lifetime of photo-generated charge carriers [15], the coupling of semiconductor systems [16–18] and the metal doping of semiconductor nanostructures [19,20]. The use of organometallic dyes like phthalocyanines and porphyrins has attracted significant attention because of their low cost and efficiency relative to the conventional solid-state conversion of visible light into chemical energy [9–12,21–25]. The main steps in a photocatalytic process mediated

* Corresponding author. Tel.: +58 4166306670.
E-mail address: onunez@usb.ve (O. Núñez).

http://dx.doi.org/10.1016/j.apcatb.2014.02.045
0926-3373/

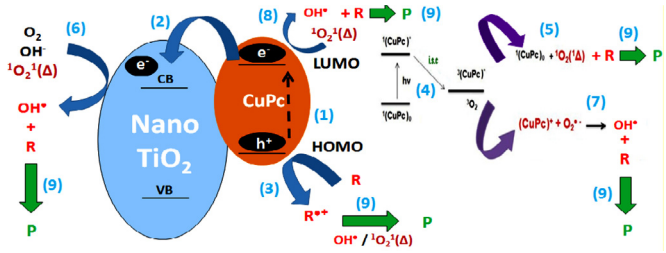

Scheme 1. Main oxidation processes involved in a photo (visible light) catalytic process mediated by TiO_2/CuPc nanoparticles.

by TiO_2-phthalocyanine nanoparticles, for instance TiO_2/CuPc, are presented in Scheme 1: (1) A macrocycle compound attached to the TiO_2 surface absorbs visible light, thereby (2) promoting electron injection into the TiO_2 conduction band [9,22,24]. (3) direct oxidation of the organic compound, (4) internal cross systems processes at the excited dye, (5) singlet oxygen formation by the interaction of dye in an excited triplet state with molecular oxygen, (6) hydroxyl radical formation [9,22] by the reduction of dissolved oxygen, hydroxyl anion and singlet oxygen, (7) hydroxyl radical formation by the reaction between the superoxide radical with the sensitizer cation [13], (8) hydroxyl radical formation by the reduction singlet oxygen at the sensitizer and (9) environmental global reaction: organic compound oxidation by the two main oxidants: hydroxyl radicals and singlet oxygen.

The photoinduced degradation of organic compounds with dye-sensitized TiO_2 nanocatalysts under visible light irradiation has been tested using synthetic contaminated effluent. This method induces an important decrease in the organic load and toxicity of wastewater. Total organic carbon (TOC) and oxygen chemical demand (COD) have been used to track organic matter mineralization. A total reduction in these parameters is a goal of practical applications. However, less effort has been done on measuring the kinetic parameters of environmental pollutant degradation and mineralization. Knowledge of these parameters permits investigators to establish the reaction mechanisms and optimal reaction conditions needed to properly describe the process for use in designing chemical reactors at large scales. The TiO_2/UV photocatalytic system results indicate that the degradation rate of the major organic compounds in this study follows the Langmuir–Hinshelwood (L–H) mechanism [1–3,7,8]. According to L–H, the initial pollutant concentration can be controlled in order to optimize degradation; for instance, the maximum observed rate constant is expected at low reactant concentrations. Additionally, catalyst surface competition can be predicted using the L–H model [7,26–29].

Dichlorvos (DDVP) is an organic phosphorus insecticide for use on pears, apples, corn, cotton, onions and tomatoes, among others. This insecticide is highly toxic to humans, mammals and aquatic animals. There are few studies in the literature about DDVP degradation through photo-induced oxidation. The photodegradation of DDVP with TiO_2 and ZnO catalysts under UV radiation from a high-pressure mercury vapor lamp has been published [30]. The insecticide concentration initially decreases, but the sample toxicity increases because reaction intermediates are formed. The kinetics and degradation mechanism of DDVP under TiO_2/UV-A treatment have also been reported [31,32]. The authors of this work assert that the initial concentration of the insecticide is significantly reduced.

For this study, dichlorvos water solutions were degraded and mineralized with simulated visible solar light and a TiO_2 surface sensitized by CuPc. The efficiencies of these experimental conditions were evaluated and compared to other DDVP degradation conditions using simulated solar light (UV + visible). The mechanistic and practical implications of these results are discussed.

2. Material and methods

2.1. Materials

The following reactants were used without further purification: dichlorvos (2,2-dichlorovinyl dimethyl phosphate), $C_4H_7Cl_2O_4P$, 76.2%, Insecticidas Internationales (INICA), Estado Aragua, Venezuela; copper(II) phthalocyanine-tetrasulfonic acid tetrasodium salt, $C_{32}H_{12}CuN_9Na_4O_{12}S_4$, Analytical Grade, Aldrich; titanium dioxide, TiO_2, P25 (70% Anatase, 30% Rutile), Degussa; hydrochloric acid, HCl, puriss, Riedel de Haën; sodium hydroxide, NaOH, 99%, Mallinckrodt; phosphoric acid, H_3PO_4, 87%, Riedel de Haën; potassium monobasic phosphoric acid, KH_2PO_4, 99%, Riedel de Haën; potassium dibasic phosphoric acid, K_2HPO_4, 98%, Riedel de Haën; hydrated potassium phosphate $K_3PO_4{\cdot}H_2O$, 95%, Riedel de Haën; sulfuric acid, H_2SO_4, 95–97%, Riedel de Haën; potassium dichromate, $K_2Cr_2O_7$, 99.5%, Merck; potassium hydrogen phthalate, $C_8H_5KO_4$, 99.5%, Riedel de Haën; water, H_2O, 17.7 MΩ cm, Nanopure.

2.2. Equipment

A Solar Light Co. solar light simulator model LS 1000 with a 1000 W xenon lamp and the appropriate filters for producing visible (400–900), UV (290–400) or UV + visible (290–900) light was used in the experiments. Solar light radiometer model PMA2100 and Ocean Optics fiber optic spectrometer model S1024dw were used to determine the radiation intensity and simulated spectra during each trial. Solution pHs were recorded with pH-meter model 713 from Metrohm. Millipore filtration equipment with 0.22, 0.20 and 0.05 μm membrane filters was used to separate TiO_2 from the sample solutions. A diode arrangement UV–vis spectrophotometer by Hewlett Packard (model HP8452A) was used to obtain the UV–vis DDVP spectrum. A Fourier-transform infrared spectrometer Bruker, model Tensor 27 was used to characterize TiO_2–CuPc interactions. An Ocean Optics spectrometer (model S1024dw) coupled with an Analytical Instruments Systems AIS (model UV-2D) light source and specular reflectance accessory with a 90° incidence (1/4 in. reflection probe model R200-7-UV/VIS) was used to obtain the TiO_2–CuPc UV–vis reflectance spectra. The Cu in solution was monitored with an ICP-AES (Inductively Coupled Plasma-Absorption Emission Spectroscope), GBC, model X2000. Oxygen singlet experiment was performed using Water Association HPLC system: M6000A pump, a Ryhodine injector, 484 UV detector and a 745B data recorder.

2.3. Methods

2.3.1. TiO_2 modification with copper(II) phthalocyanine-tetrasulfonic acid tetrasodium salt (CuPc)

A titanium dioxide surface was modified with CuPc using the liquid–solid adsorption-equilibrium method. The general procedure consisted of mixing 200 mg of TiO_2 with 50 mL of CuPc aqueous solutions at different concentrations in neutral pH media. The mixtures were magnetically stirred until adsorption equilibrium was reached. This equilibrium was monitored by measuring the CuPc UV–vis absorbance of previously filtered aliquots. In all cases, equilibrium was reached in 15 days. The amount of CuPc adsorbed on the TiO_2 surface was calculated by taking the difference between the initial and remaining CuPc concentrations in solution. The analytical quantification of CuPc was performed using the UV–vis spectra and calibration curves according to the Lambert–Beer law. For CuPc, the extinction coefficient at 238 nm is

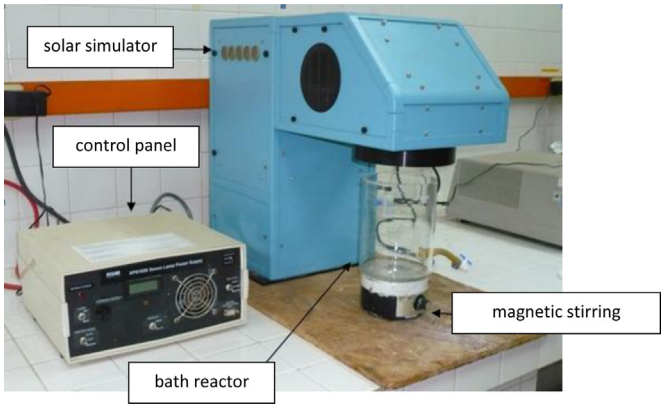

Scheme 2. Experimental set up for Dichlorvos photocatalytic oxidation.

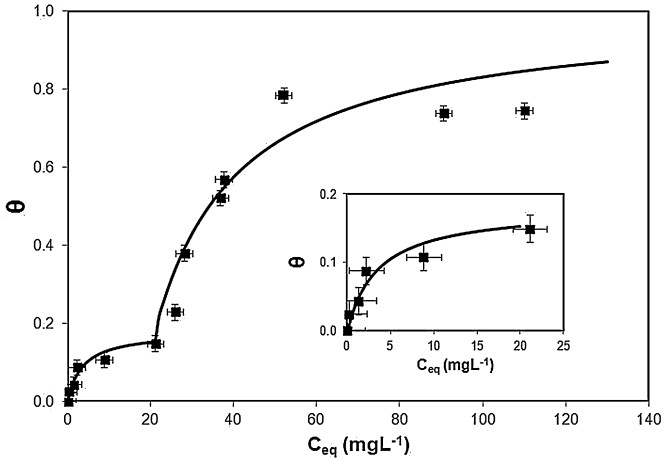

Fig. 1. CuPc adsorption isotherm on TiO_2 surface. (■) Experimental results. (—) Fit to multi-site Langmuir isotherms. Error bars: $x \pm 2$ and $y \pm 0.015$.

$0.067\ L\ mg^{-1}\ cm^{-1}$. The adsorption isotherms were obtained from plots of surface-adsorbed CuPc per gram of TiO_2 added vs. the CuPc equilibrium concentration. The adsorption equilibrium constants (K_i) and the maximum amount of CuPc adsorbed (Q_i) during the different TiO_2–CuPc interactions were obtained from a best fit of a multi-site Langmuir isotherm [33] to the resulting experimental points. The modified TiO_2 was separated from the solution and washed with 5 mL of water and stored in a dry vessel. FTIR and UV–vis reflectance spectra were used to characterize the TiO_2–CuPc interactions and light absorbance. The new catalyst was used in the visible light photocatalytic oxidation of DDVP.

2.3.2. Dichlorvos photocatalytic oxidation

In a 600 mL borosilicate beaker with a magnetic stirrer, a suspension of 250 mL of DDVP and phosphate buffer solution (pH 7) with 100 mg L^{-1} of the TiO_2-CuPc photocatalyst was prepared. This suspension remained in the dark for 30 min in order to establish the reactant-TiO_2 adsorption/desorption equilibrium. After this time, the system was placed under a solar simulator cannon (diameter ca. 20 cm) in such a way that the distance between the end of the cannon and the beaker was 15 cm (see Scheme 2). The simulator was turned on, and the reaction was monitored by taking aliquots (3 mL) at different times. The aliquots were filtered with Millipore membranes, and the UV–vis spectrum of the filtered solution was recorded. DDVP analytical quantification was performed with the UV–vis spectra and calibration curves according to the Lambert–Beer law (the extinction coefficient for DDVP at 206 nm was $0.091\ L\ mg^{-1}\ cm^{-1}$). Simulator radiation was measured with a radiometer. Values of ca. 90 mW cm^{-2} were typically measured for visible radiation. The temperature of the reactor was kept at $22 \pm 1\ ^\circ C$ by maintaining the temperature of the room where the simulator was located.

An argon ICP-AES spectrophotometer was used to evaluate the stability of the Cu-modified catalyst after three hours of visible light irradiation, resulting in 20 mg L^{-1} UV–vis degradation of DDVP. No Cu was found in any of the analyzed solutions. The corresponding filtered and modified catalysts were dried and analyzed with UV–vis reflectance. The resulting spectra were identical to the spectrum of the unused catalyst. Therefore, there was no Cu release into the solutions or catalyst degradation under these experimental conditions.

2.3.3. Numerical analysis

Linear fits were performed with a traditional least squares algorithm. Nonlinear least squares fits were realized with Matlab v. 7.0 using Trust-Region and Levenberg–Marquardt algorithms; these routines were considered in robust and non-robust methods, with a non-negative iteration of the fitting parameters. The resulting kinetic values were corroborated by ANOVA statistics using Statgraphics v. 5.1. The results were considered statistically different with confidence intervals of 95%. The error bars demonstrated the estimated maximum error of the variable domain.

2.3.4. Singlet oxygen and hydroxyl radical trapping experiments

TiO_2-CuPc-in water was irradiated with simulated visible light. Singlet oxygen $^1O_2{}^1(\Delta)$ was trapped with 1,3-ciclohexadiene-1,4-diethanoate (0.5 mM). After 60 min irradiation a sample was taken and analyzed with a HPLC provided with an UV detector. A reverse-phase column (C-18) and CH_3OH:H_2O:H_3PO_4 (40:60:0.2) as eluyent with an injection flux of 1.0 mL min^{-1} was used. 20 μL of sample at 25 °C were injected. The adduct (endoperoxide of the 1,3-ciclohexadiene) is formed via diene + $^1O_2$ pericyclic reaction. It was detected at a retention time of 4.2 min using an UV detector in the range 200–270 nm. The oxygen singlet concentration is ca. 0.3 mM (9.6 mg L^{-1}). Hydroxyl radical was trapped using *N*,*N*-dimetil-p-nitrosoanilina (1 ppm). Significant decreasing ca. 25% of the UV–vis absortion intensity of the last compound at 440 nm was observed after 60 min irradiation.

2.3.5. Mineralization

Mineralization during DDVP photocatalytic oxidation was followed by measuring the chemical oxygen demand (COD). In a typical reaction, aliquots (3 mL) were taken at different reaction times and the COD of each aliquot was measured with a colorimetric method [34] in which the total organic sample content was oxidized for 2 h at 150 °C in a closed system with sulfuric acid and potassium dichromate. The solution absorbance at 420 and 600 nm were then measured. From this absorbance, the solution COD was obtained from a potassium hydrogen phthalate calibration curve.

3. Results and discussion

3.1. Langmuir Isotherms

In Fig. 1, the adsorption isotherms of copper(II) phtalocyanine-tetrasulfonic acid tetrasodium salt (CuPc) on TiO_2 Degussa P25 at a neutral pH are shown. In Fig. 1, the multi-site Langmuir isotherms have been fitted (solid line) to the experimental data. Two consecutive Langmuir isotherms describe the TiO_2 surface coverage. The first Langmuir isotherm reaches a maximum CuPc adsorption (first leveling, see zoom in Fig. 1) at 8 mg g^{-1} ($\theta = 18\%$), and the second one is at 39 mg g^{-1} ($\theta = 82\%$). Although levels reach maximum at $\theta = 18\%$ and $\theta = 82\%$ respectively, samples with coverage

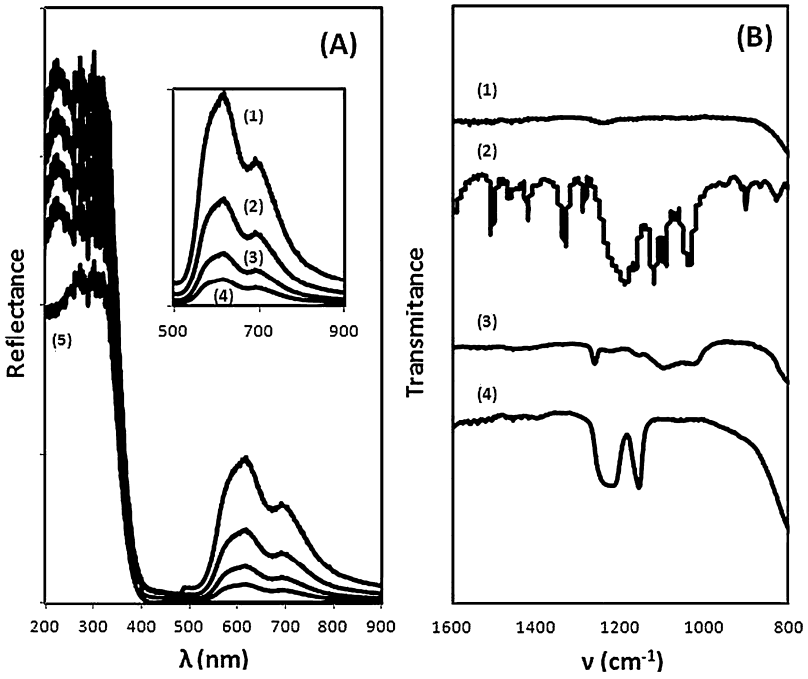

Fig. 2. (A) UV–vis reflectance spectra of TiO_2 (5) and TiO_2-CuPc: (4) $\theta = 4\%$ *y* (3) $\theta = 9\%$, (2) $\theta = 34\%$ and (1) $\theta = 79\%$. (B) FTIR spectra of TiO_2 (1), CuPc (2) and TiO_2–CuPc interactions: (3) $\theta = 79\%$ and (4) $\theta = 9\%$.

at $\theta = 9\%$ and $\theta = 79\%$ (starting of each level) were used as representative of these two conditions in the rest of the experiments. Fig. 1 fitting indicates CuPc adsorption–desorption equilibrium constants of $K_1 = 0.28\,L\,mg^{-1}$ and $K_2 = 0.05\,L\,mg^{-1}$. Although there is less coverage (θ) in the first Langmuir, its adsorption–desorption equilibrium constant value is greater than the second Langmuir. Fig. 2 shows the UV–vis reflectance and IR spectra of TiO_2/CuPc, TiO_2 and CuPc samples. In Fig. 2A, the TiO_2/CuPc samples correspond to different θ values, and Fig. 2B indicates $\theta = 9\%$ and 79%, representing the θ of the two levels in Fig. 1. In Fig. 2A, UV–vis reflectance absorption bands at 600 and 700 nm confirm the presence of CuPc on the TiO_2 surface. TiO_2 does not absorb in the visible. In the IR spectrum shown in Fig. 2B, the —S—O—Ti— characteristic stretching signals at 1150 and 1210 cm^{-1} (see 2B (4)) suggest chemical CuPc adsorption via Ti–OH and CuPc–sulfonic acid bond formation ($TiO–SO_3^-$) [35]. The intensities of these signals are quite a bit higher than the corresponding maximum CuPc coverage from the second Langmuir that appear at 1160 and 1260 cm^{-1} (see 2B(3)) This observation supports the suggestion that there are more —S—O—Ti— bonds involved in the first case, meaning that each CuPc adsorbed at the TiO_2 surface is anchored using two or more sulfonic acid moieties (Scheme 3). Therefore, the CuPc molecules may have more planar distribution on the TiO_2 surface relative to the second Langmuir case, in which the high coverage prevents CuPc molecule multi-anchoring at the TiO_2 surface. This observation is in agreement with a higher adsorption–desorption K_1 value for the first Langmuir and also with the two IR bands at 1010 and 1070 cm^{-1} that are characteristic of C—H CuPc macrocycle-ring bending. These bands are more important in spectrum 2B(3) ($\theta = 79\%$), where there is less parallel CuPc molecule distribution on the TiO_2 surface than in 2B(4) ($\theta = 9\%$) and consequently less impediment to bending.

3.2. Dichlorvos (DDVP) photocatalytic degradation

Fig. 3 shows DDVP photoinduced degradation at pH 7 (phosphate buffer) with simulated visible solar light and TiO_2/CuPc ($\theta = 9\%$) as the catalyst. Fig. 3A shows the DDVP UV spectra at different reaction times. The UV band at 206 nm, which is shown in the figure, was used to obtain the DDVP concentrations at each reaction time. In Fig. 3B, the first-order DDVP degradations at different initial concentrations are shown. An exponential first-order reaction rate equation was fit (continuous line) to the experimental points at each concentration in order to obtain the corresponding pseudo-first-order rate constants. As shown in Fig. 3B, the reaction becomes faster when the initial DDVP concentration is lower. This observation is in agreement with the L–H kinetic model-derived reaction rate:

$$rate = \frac{k_{DDVP}K_{DDVP}C_{DDVP}}{1 + K_{DDVP}C_{DDVP}} = k_{obs}C_{DDVP} \quad (1)$$

where

$$k_{obs} = \frac{k_{DDVP}K_{DDVP}}{1 + K_{DDVP}C_{DDVP}} \quad (2)$$

Therefore, DDVP must approach the catalyst, and a proportion of it adheres to the catalyst surface establishing an adsorption equilibrium (K_{DDVP} ($L\,mg^{-1}$)), where it degrades. Its limiting degradation rate at maximum coverage is given

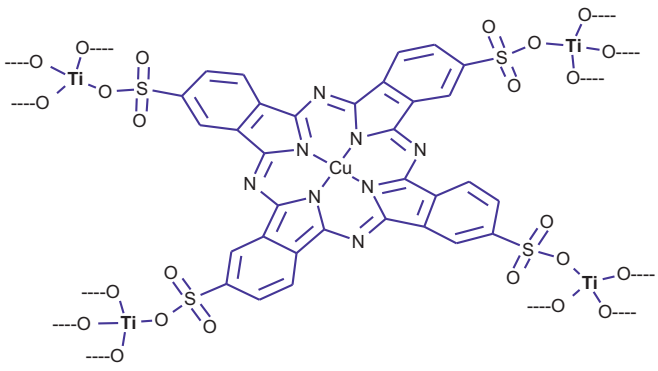

Scheme 3. Chemical CuPc absorption on the TiO_2 surface. Multiple —SO_3—O—Ti— interactions per CuPc molecule induce a CuPc planar distribution on the TiO_2 surface.

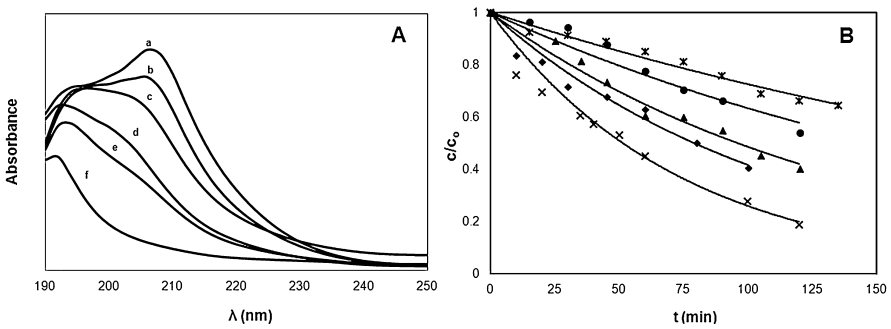

Fig. 3. (A) DDVP spectra decay during the TiO_2/CuPc photo-induced process. Sample times: (a) 0 min, (b) 30 min, (c) 75 min, (d) 90 min, (e) 120 min, (f) 210 min. (B) Concentration vs. time for DDVP degradation at different initial concentrations. (x) 5.05 mg L^{-1}; (♦) 13.90 mg L^{-1}; (▲) 24.09 mg L^{-1}; (●) 32.01 mg L^{-1}; (Ж) 35.94 mg L^{-1}; (—) Fit to pseudo-first-order kinetics. [TiO_2/CuPc] = 100 mg L^{-1} (θ = 9%). pH 7 (phosphate buffer). T = 22 °C.

by k_{DDVP} (mg L^{-1} min^{-1}). According to the previous equations, ($1 > K_{DDVP}C_{DDVP}$), rate = $k_{DDVP}K_{DDVP}C_{DDVP}$ and $k_{obs} = k_{DDVP}K_{DDVP}$ at low C_{DDVP}, meaning that a rate increase must be observed in concert with a [DDVP] increase. However, at relatively high C_{DDVP}, $1 < K_{DDVP}C_{DDVP}$ and the rate (rate = k_{DDVP}, Eq. (1)) reaches a maximum level. As described, a rate increase is observed at low C_{DDVP} but a rate decrease (see Fig. 4) is obtained when increasing C_{DDVP} even more, instead of the expected leveling (rate = k_{DDVP}). This inhibition can be explained in terms of Scheme 1 with the participation of oxygen. In fact, O_2 may participate via four different mechanisms marked as (5)–(8) in Scheme 1. All of them require water in order to have dissolved oxygen at the catalyst surface for promoting DDVP degradation. Therefore, these mechanisms have a general L–H $rate = k_{O_2}K_{O_2}C_{O_2}/(1 + K_{DDVP}C_{DDVP} + K_{O_2}C_{O_2})$. This equation predicts an inhibition of the O_2 contribution rate when C_{DDVP} increases because of its competition for sites at the catalyst surface. In fact, this inhibition is observed in Fig. 4. Combining the different contributions for DDVP degradation according to Scheme 1, we deduced a long equation (see Section 3.3) that we have adjusted to the experimental points in Fig. 4 [36].

3.3. Kinetic Model: visible light photoinduced degradation of organic compounds on phthalocyanine-sensitized TiO_2: fitting the bell-shaped kinetics to the experimental points

Modified TiO_2 reactions with organometallic sensitizers such as phthalocyanines and porphyrins have been studied by Mele et al. [9]. This mechanism includes several reactions; however, some of them can be very fast and do not limit the global reaction [2,37,38].

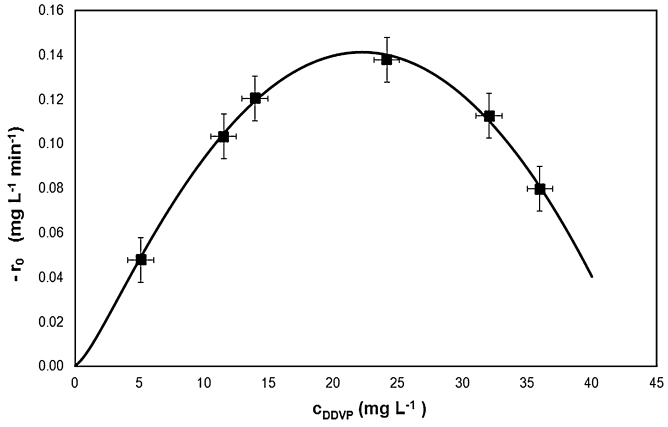

Fig. 4. Bell shape profile in the rate vs. dichlorvos concentration for the TiO_2/CuPc photo-induced oxidation. [TiO_2/CuPc] = 100 mg L^{-1} (θ = 9%). pH 7 (phosphate buffer). T = 22 °C. Solid line: best fit using Eq. (14). Error bars: $x \pm 2$ and $y \pm 0.008$.

Therefore, the following rate law considers only the limited participation of hydroxyl radicals and singlet oxygen as oxidant agents.

The organic compound and molecular oxygen interact via adsorption–desorption equilibrium on the surface of the sensitized catalyst (TiO_2-S[]) as shown in Eqs. (3) and (4).

$$R + TiO_2 - S[] \underset{}{\overset{K_g}{\rightleftharpoons}} TiO_2 - S[R] \quad (3)$$

$$O_2 + TiO_2 - S[] \underset{}{\overset{K_{O_2}}{\rightleftharpoons}} TiO_2 - S[O_2] \quad (4)$$

After visible solar light absorption, an electron on the semiconductor (TiO_2) conduction band (CB) and a hole on the HOMO of the sensitizer are formed. These additions allow the formation of hydroxyl radicals according to Scheme 1. These radicals are formed via molecular O_2 reduction on the semiconductor surface via peroxide radicals [2,22] (Eq. (5)) and singlet oxygen generation [4] on the excited sensitizer (Eq. (6)).

$$TiO_2 - S[O_2] + e^-_{CB} \rightarrow TiO_2 - S\left[O_2^-\right] \rightarrow\rightarrow TiO_2 - S[OH\bullet] \quad (5)$$

$$TiO_2 - {}^3S^*[] + O_2 \rightarrow TiO_2 - S[] + {}^1O_2({}^1\Delta) \quad (6)$$

These two oxidant agents react with organic compounds to yield the oxidized products, which are then further mineralized (Eqs. (7) and (8)).

$$TiO_2 - S[OH\bullet] + TiO_2 - S[R] \rightarrow P_1 \overset{OH\bullet}{\longrightarrow} \overset{{}^1O_2({}^1\Delta)}{\longrightarrow} CO_2 + H_2O + MA \quad (7)$$

$${}^1O_2({}^1\Delta) + TiO_2 - S[R] \rightarrow P_2 \overset{OH\bullet}{\longrightarrow} \overset{{}^1O_2({}^1\Delta)}{\longrightarrow} CO_2 + H_2O + MA \quad (8)$$

The proposed rate law considers the organic oxidation to occur via the two main contributions of the radical hydroxyl and singlet oxygen as it is describe in routes 9 of Scheme 1. In fact, by irradiating TiO_2-CuPc catalyst in water with visible light we have verified the production of singlet oxygen and hydroxyl radical via trapping experiments. We have used 1,3-ciclohexadiene-1,4-diethanoate (0.5 mM) to trap singlet oxygen [44] and detected the adduct formed via HPLC (UV detector) with a retention time of 4.2 min. The hydroxyl radical was trapped [45] using *N*,*N*-dimetil-p-nitrosoaniline (1 ppm). Reduction of the last compound signal at λ_{max} = 440 nm, verified hydroxyl radical formation in solution. These two radicals are the basis for this section equations derivation. Therefore, reaction rate depends on both species as shown in Eq. (9).

$$r_o = k_{R-OH}\theta_{OH}\theta_R + k_{R-OS}C_{OS}C_R \quad (9)$$

where r_o is the reaction rate, k_{R-OH} is the rate constant of the organic degradation at the catalyst surface, k_{R-OS} is the second-order rate constant between the organic compound and the singlet oxygen, C_{OS} is the last species concentration and C_R is the organic compound concentration. Although the last term refers to a reaction in

solution, the oxygen must approach the catalyst surface in order to produce C_{OS}. The θ_R and θ_{OH} are the organic and hydroxyl radical fractions on the catalyst surface, respectively. These fractions can be described according to Langmuir-adsorption isotherms as follows:

$$\theta_R = \frac{K_R C_R}{1 + K_R C_R + K_{O_2} C_{O_2}} \quad (10)$$

$$\theta_{O_2} = \frac{K_{O_2} C_{O_2}}{1 + K_R C_R + K_{O_2} C_{O_2}} \quad (11)$$

where C_{O_2} is the dissolved oxygen concentration and K_R and K_{O_2} are the Langmuir adsorption constants of the organic compound and oxygen on the catalyst.

The change in hydroxyl radical concentrations is given by Eq. (12):

$$\frac{dC_{OH}}{dt} = k_A C_{e^-}\theta_{O_2} + k_B \Gamma_S \theta_{O_2} + k_C \Gamma_S C_{OH^-} + k_D C_{e^-} C_{OS} + k_E \Gamma_S C_{OS} - k_{R-OH}\theta_{OH}\theta_R - k_R \theta_{OH} - k_F \quad (12)$$

where k_i are the kinetic rate constants, C_{e^-} is the electron concentration on the catalyst conduction band, C_{OH^-} is the hydroxyl ion solution concentration, C_{OS} is the concentration of singlet oxygen and Γ_s is the sensitizer catalyst surface concentration. The first five terms in Eq. (12) correspond to radical hydroxyl production from oxygen reduction from electrons at the catalyst conduction band ($k_A C_{e^-}\theta_{O_2}$), oxygen reduction at the sensitizer adsorbed on the TiO_2 ($k_B \Gamma_S \theta_{O_2}$), hydroxyl ion reduction by the sensitizer adsorbed on the TiO_2 ($k_C \Gamma_S C_{OH^-}$), singlet oxygen reduction by the electrons at the TiO_2 conduction band ($k_D C_{e^-} C_{OS}$) and oxygen reduction at the sensitizer as adsorbed on the TiO_2 ($k_E \Gamma_S C_{OS}$). The consumption of hydroxyl radicals (last three terms in Eq. (12)) correspond to its depletion by its reaction with the organic pollutant ($k_{R-OH}\theta_{OH}\theta_R$), the recombination reaction with water ($k_R\theta_{OH}$) and the formation of other oxygenated species (k_F).

Steady-state of the hydroxyl radical gives Eq. (13):

$$\theta_{OH} = \frac{(k_A C_{e^-} + k_B \Gamma_S)\theta_{O_2} + k_C \Gamma_S C_{OH^-} + k_D C_{e^-} C_{OS} + k_E \Gamma_S C_{OS} - k_F}{k_R + k_{R-OH}\theta_R} \quad (13)$$

where the C_{OS} is constant [39,40] and depends on the amount of sensitizer at the catalyst surface.

Finally, substituting Eq. (10), (11) and (13) in Eq. (9), the following rate law has constant terms grouped together in order to simplify the equation.

$$r_o = k_{R-OH}\left[\frac{(k_A C_{e^-} + k_B \Gamma_S)\left(\frac{K_{O_2} C_{O_2}}{1+K_{O_2} C_{O_2}+K_R C_R}\right) + k_C \Gamma_S C_{OH^-} + k_D C_{e^-} C_{OS} + k_E \Gamma_S C_{OS} - k_F}{k_R + k_{R-OH}\left(\frac{K_R C_R}{1+K_{O_2} C_{O_2}+K_R C_R}\right)}\right]\left(\frac{K_R C_R}{1 + K_{O_2} C_{O_2} + K_R C_R}\right) + k_{R-OS} C_{OS} C_R \quad (14)$$

The following three parameters are relevant in Eq. (14): the limiting rate constant (rate units) between organic and hydroxyl radicals (k_{R-OH}), the rate constant term (second-order rate constants units) from the interaction between the organic compound and the singlet oxygen (k_{R-OS}) and the organic equilibrium adsorption constant on the modified catalyst surface (K_R). The other constants in Eq. (14) have been determined in previous studies [2,39–43]. Finally, as shown in Fig. 4, the experimental points of a rate vs. C_{DDVP} plot with a theoretical curve are described by Eq. (14). From the fitting of the last equation to the experimental data, the $K_{DDVP} = 0.016\ L\ mg^{-1}$, the DDVP limiting degradation rate from hydroxyl radicals $k_{DDVP\text{-}OH.} = 1.09\ mg\ L^{-1}\ min^{-1}$, and the singlet oxygen-DDVP second order rate constant $k_{DDVP\text{-}OS} = 0.45\ L\ mg^{-1}\ min^{-1}$ (see Table 1). The results for the rate constants are summarized in Table 1.

Table 1
Rate constant for dichlorvos photoinduced degradation by visible solar light on TiO_2-CuPc ($\theta = 9\%$).

Rate constant	Value
k_{R-OH} ($mg\ L^{-1}\ min^{-1}$)[a]	1.09
k_{R-OS} ($L\ mg^{-1}\ min^{-1}$)[a]	0.45
K_R ($L\ mg^{-1}$)[a]	0.016
$k_A C_{e^-}$ ($mg\ L^{-1}\ min^{-1}$)[b]	111
$k_B \Gamma_s$ ($mg\ L^{-1}\ min^{-1}$)[b]	47
$k_C \Gamma_s c_{OH^-}$ ($mg\ L^{-1}\ min^{-1}$)[b]	6
$k_D c_e - c_{OS}$ ($mg\ L^{-1}\ min^{-1}$)[b]	21
$k_E \Gamma_s c_{OS}$ ($mg\ L^{-1}\ min^{-1}$)[b]	14
k_F ($mg\ L^{-1}\ min^{-1}$)[b]	125
k_R ($mg\ L^{-1}\ min^{-1}$)[b]	9.50
K_{O_2} ($L\ mg^{-1}$)[b]	0.10

[a] Obtained from non-linear fit of Eq. (14) to the experimental data represented in Fig. 4.
[b] Estimated from Refs. [2,39].

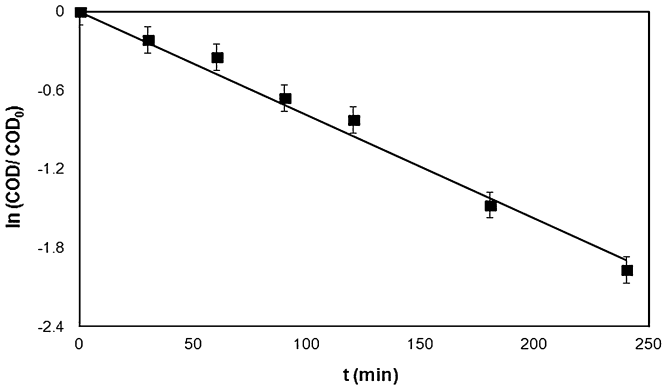

Fig. 5. $\ln(COD/COD_0)$ vs. time of the photo-induced DDVP degradation for the TiO_2/CuPc catalyst ($\theta = 9\%$). Initial $C_{DDVP} = 24.09\ mg\ L^{-1}$. pH 7 (phosphate buffer). $T = 22\ ^\circ C$. Error bars: $y \pm 0.07$.

3.4. Dichlorvos (DDVP) photocatalytic mineralization

In Fig. 5, DDVP mineralization kinetics were obtained at pH 7 (phosphate buffer) using $100\ mg\ L^{-1}$ of TiO_2/CuPc ($\theta = 9\%$) and simulated visible solar light. A $k_{obs} = 0.0079\ min^{-1}$ was found using the slope of the straight line. Under the same experimental conditions, DDVP degradation was followed and a $k_{obs} = 0.0072\ min^{-1}$ was found from the slope of the $\ln C_{DDVP}$ vs. t plot. This finding indicates that both mineralization and degradation processes have the same rate limiting step. Therefore, there is no intermediate accumulation during the DDVP treatment under the described conditions. This is important because it was reported [30] that toxic intermediates form when TiO_2/UV light is used to degrade DDVP. The oxygen singlet contribution toward the oxidation process makes all the difference in this work, probably because of its concentration (ca. 0.3 mM ($9.6\ mg\ L^{-1}$)), from trapping experiment) and oxidant capacity since oxygen is ca. 1 V more oxidizing in its singlet excited state. Since the $9.6\ g\ mg\ L^{-1}$ of singlet oxygen was consumed in ca. 1 h, the expected rate would be $0.16\ mg\ L^{-1}\ min^{-1}$ ($9.6\ mg\ L^{-1}/60$ min). This number is in good agreement with Fig. 4 maximum rate.

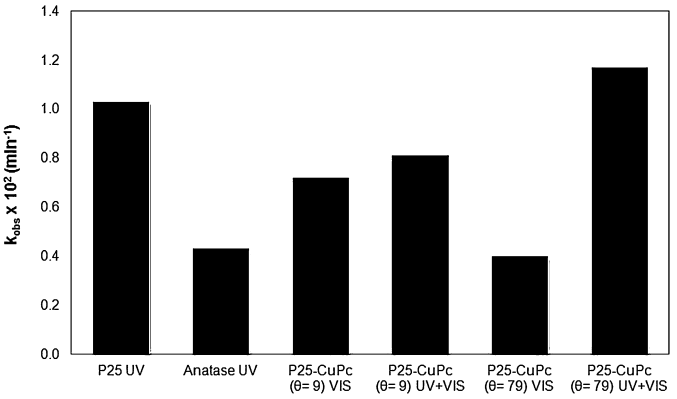

Fig. 6. Pseudo-first-order rate constants under different conditions for TiO_2 photo-induced DDVP degradation. In all cases, standard deviation < 5% (3 subsamples).

3.5. 3.5. DDVP degradation rate constants under different conditions of simulated solar light irradiation

In Fig. 6, the DDVP degradation k_{obs} values from simulated solar visible light TiO_2/CuPc (θ = 9%) and TiO_2/CuPc (θ = 79%) were compared with other TiO_2 photocatalytic induced DDVP degradation from simulated solar light. These k_{obs} are really constants ($k_{obs} = kK_{DDVP}$) and independent of C_{DDVP}, as the condition $1 > K_{DDVP}C_{DDVP}$ (see Eq. (14)) holds true in all cases. Therefore, these rate constants can be compared in order to estimate the relative degradation rates. The maximum value of $k_{obs} = 0.011\ min^{-1}$ was obtained when TiO_2 Degussa P25/CuPc (θ = 79%), UV + visible solar light was used, and the minimum was achieved when the same catalyst was irradiated with visible simulated solar light alone. Therefore, high CuPc TiO_2 surface coverage decreases O_2 oxidation (sensitization via visible light) but increases the water's approach to the catalyst surface, probably because of a less even distribution of CuPc molecules on the catalyst surface. In fact, when UV + visible simulated light was used on the low coverage (θ = 9%) TiO_2/CuPc catalyst, the resulting k_{obs} was lower than the high coverage trial (θ = 79%). Indeed, in the θ = 9% case, the UV activation was less effective as a result of parallel CuPc distribution, which limited the water's approach and the formation of hydroxyl radicals.

4. Conclusions

A modified TiO_2 surface using CuPc at low coverage conditions (θ = 9%) induces effective DDVP degradation and mineralization when visible solar simulated light is used. There is not risk of Cu contamination when using TiO_2/CuPc catalyst during this DDVP mitigation. There was also no accumulation of DDVP degradation intermediates. The parallel distribution of CuPc molecules on the TiO_2 surface promotes O_2 degradation, contributing to sensitization as follows: O_2 triplet $\rightarrow$ O_2 singlet + DDVP. However, this mechanism was inhibited at high C_{DDVP}. In fact, an unusual bell-shaped profile was obtained in a plot of the DDVP degradation rate vs. C_{DDVP}. Although sensitization was promoted under the last condition at low C_{DDVP}, UV $OH^{\bullet}$ generation was lessened because of limitations in water's approach to the catalyst surface. The final degradation mechanism was less inhibited at high CuPc coverage (θ = 79%) due to the less planar reactant distribution on the TiO_2 surface. As a consequence, the fastest DDVP degradation was observed with the final catalyst and simulated solar light (UV + visible light).

Acknowledgements

We acknowledge UGA-USB (Unidad de Gestión Ambiental from Universidad Simón Bolívar) for its financial support. We are also grateful to Gilberto Geller and Diego Aliso at the Universidad Simón Bolívar for technical assistance and to Prof. Edgardo Leal from Universidad Central de Venezuela for his collaboration.

References

[1] D. Ollis, Environ. Sci. Technol. 19 (1985) 480–484.
[2] M. Hoffmann, S. Martin, W. Choi, D. Bahnemann, Chem. Rev. 95 (1995) 69–96.
[3] U.I. Gaya, A.H. Abdullah, J. Photochem. Photobiol. C: Photochem. Rev. 9 (2008) 1–12.
[4] M. Henderson, Surf. Sci. Rep. 66 (2011) 185–297.
[5] I. Muñoz, J. Rieradevall, F. Torrades, J. Peral, X.X. Doménech, Solar Energy 79 (2005) 369–375.
[6] S. Malato, J. Blanco, D.C. Alarcón, M.I. Maldonado, P. Fernandez-Ibáñez, W. Gernjak, Catal. Today 122 (2007) 137–149.
[7] R. Vargas, O. Núñez, Solar Energy 84 (2010) 345–351.
[8] M.A. Fox, M.T. Dulay, Chem. Rev. 93 (1993) 341–357.
[9] G. Mele, R. Del Sole, G. Vasapollo, E. García-López, L. Palmisano, M. Schiavello, J. Catal. 217 (2003) 334–342.
[10] V. Iliev, J. Photochem. Photobiol. A: Chem. 151 (2002) 195–199.
[11] V. Iliev, D. Tomova, L. Bilyarska, L. Prahov, L. Petrov, J. Photochem. Photobiol. A: Chem. 159 (2003) 281–287.
[12] Z. Wang, W. Mao, H. Chen, F. Zhang, X. Fan, G. Qian, Catal. Commun. 7 (2006) 518–522.
[13] R. Vinu, S. Polisetti, G. Madras, Chem. Eng. J. 165 (2010) 784–797.
[14] P. Wen, S. Yang, Y. Ishikawa, H. Itoh, Q. Feng, Appl. Surf. Sci. 257 (2011) 2126–2133.
[15] N. Ortega, O. Núñez, Avances en Ciencias e Ingeniería 3 (1) (2012) 81–91.
[16] M. Abou Asi, C. He, M. Su, D. Xia, L. Lin, H. Deng, Y. Xiong, R. Qiu, X-Z. Li, Catal. Today 175 (2011) 256–263.
[17] J. Li, Y. Yu, Z. Liu, S. Zuo, B. Li, Int. J. Photoenergy 2012 (2012) 7, http://dx.doi.org/10.1155/2012/254201, Article ID 254201.
[18] Z. Liu, X. Xu, J. Fang, X. Zhu, J. Chu, B. Li, Appl. Surf. Sci. 258 (2012) 3771–3778.
[19] V. Iliev, D. Tomova, S. Rakovsky, A. Eliyas, G. Li Puma, J. Mol. Catal. A: Chem. 327 (2010) 51–57.
[20] D. Tomova, V. Iliev, S. Rakovsky, M. Anachkov, A. Eliyas, G. Li Puma, J. Photochem. Photobiol. A: Chem. 231 (2012) 1–8.
[21] C. Wang, J. Li, G. Mele, G-M. Yang, F-X. Zhang, L. Palmisano, G. Vasapollo, Appl. Catal. B: Environ. 76 (2007) 218–226.
[22] A. Machado, M. França, V. Velani, G. Magnino, H. Velani, F. Freitas, P. Müller, C. Sattler, M. Schmücker, Int. J. Photoenergy 2008 (2008) 12, http://dx.doi.org/10.1155/2008/482373, Article ID 482373.
[23] C. Wang, J. Li, G. Mele, M-Y. Duan, X-F. Lü, L. Palmisano, G. Vasapollo, F-X. Zhang, Dyes Pigments 84 (2010) 183–189.
[24] H. Shibata, S. Ohshika, T. Ogura, S. Watanabe, K. Nishio, H. Sakae, M. Abe, K. Hashimoto, M. Matsumoto, J. Phothochem. Photobiol. A: Chem. 217 (2011) 136–140.
[25] D. Oliveira, P. Batista, P. Muller, V. Velani, M. França, D. De Souza, A. Machado, Dyes Pigments 92 (2012) 563–572.
[26] R. Vargas, O. Núñez, J. Mol. Catal. A: Chem. 300 (2009) 65–71.
[27] G. Pardo, R. Vargas, O. Núñez, J. Phys. Org. Chem. (2008) 1072–1078.
[28] R. Vargas, O. Núñez, J. Mol. Catal. A: Chem. 294 (2008) 74–81.
[29] I. Kuehr, O. Núñez, Pest Manage. Sci. 63 (2007) 491–494.
[30] E. Evgenidou, K. Fytianos, I. Poulios, Appl. Catal. B: Environ. 59 (2005) 81–89.
[31] P. Oancea, T. Oncescu, J. Photochem. Photobiol. A: Chem. 199 (2008) 8–13.
[32] T. Oncescu, M.I. Stefan, P. Oancea, Environ. Sci. Pollut. Res. 17 (2010) 1158–1166.
[33] P. Grant, S. Lemke, M. Dwyer, T. Phillips, Langmuir 14 (1998) 4292–4299.
[34] A.L. Greenberg, A.E. Clesceri, Standard Methods for the Examination of Water and Wastewater, Eighteen ed, American Public Health Association, American Water Works Association, Waste Environment Federation, USA, 1992.
[35] T. Ma, Y. Wei, T. Ren, L. Liu, Q. Guo, Z.Z. Yuan, Appl. Mater. Interfaces 2 (2010) 3563–3571.
[36] E. Vargas, Fotocatálisis del insecticida diclorvos empleando simulación solar y TiO_2 sensibilizado con ftalocianina de cobre, Bachelor in Chemistry Thesis Dissertation, Universidad Central de Venezuela, 2011, pp. 1–106.
[37] K. Vinodgopal, K.X. Hua, R.L. Dahlgren, A.G. Lappin, L.K. Patterson, P.V. Kamat, J. Phys. Chem. 99 (1995) 10883–10889.
[38] D. Friedmann, C. Mendive, D. Bahnemann, Appl. Catal. B. Environ. 99 (2010) 398–406.
[39] C. Pierlot, V. Nardello, R. Schmidt, J.-M. Aubry, ARKIVOC 8 (2007) 245–256.
[40] M.C. DeRosa, R.J. Crutchley, Chem. Rev. 233–234 (2002) 351–371.
[41] J.L. Redpath, R.L. Wilson, Int. J. Radiat. Biol. Relat. Stud. Phys. Chem. Med. 27 (4) (1975) 389–398.
[42] N.D. Popovic, D.C. Anal. Chem. 70 (1998) 468–472.
[43] H.H. Mohamed, R. Dillert, D.W. Bahnemann, J. Photochem. Photobio. A: Chem. 217 (2011) 271–274.
[44] V. Nardello, D. Brault, P. Chavalle, J-M. Aubry, J. Phothochem. Photobiol. B: Biol. 39 (1997) 146–155.
[45] Ch. Comninellis, Electrochim. Acta 39 (1994) 1857–1862.